https://doi.org/10.5194/egusphere-2026-6957
Preprint. Discussion started: 23 November 2026
© Author(s) 2026. CC BY 4.0 License.

Long-term trends and drivers of urban-nonurban $PM_{2.5}$ gap over the Yangtze River Delta, China, during 2000–2025

Ning Ruan[1], Zhen Li[1], Jie Fang[2], Jingyi Yang[1], Jianfeng Zhang[1], Wenjing Li[3], Yunjiang Zhang[2], Mindong Chen[2], Xinlei Ge[1,*]

[1] School of Energy and Environment, Southeast University, Nanjing 211189, China

[2] Jiangsu Key Laboratory of Intelligent Atmospheric Environment Monitoring and Carbon-Pollution Co-Control (IAEMCPC), School of Environmental Science and Engineering, Nanjing University of Information Science and Technology, Nanjing 210044, China

[3] Meteorological Development and Planning Institute of China Meteorological Administration, Beijing 100081, China

Correspondence to: Xinlei Ge (xinlei@seu.edu.cn)

Abstract. China's successive clean-air regulatory policies have achieved remarkable nationwide $PM_{2.5}$ decreases over the past decades. Even so, few studies have systematically quantified how urban-nonurban $PM_{2.5}$ disparities evolve alongside changing emission controls, and disentangled the respective roles of anthropogenic and meteorological drivers. Here, we took the densely populated Yangtze River Delta (YRD) as a model domain. Based on 1 km gridded $PM_{2.5}$ data, dynamic settlement masks, weather-normalized decomposition, and interpretable machine learning (ML) regression, we analyse the long-term characteristics of $PM_{2.5}$ concentrations and the urban-nonurban $PM_{2.5}$ differences for 41 YRD cities from 2000 to 2025. The urban-nonurban $PM_{2.5}$ gap switched from widening to narrowing in 2007, a few years ahead of the 2013 national clean-air action plan, dropping from a peak of 7.87 $\mu g \cdot m^{-3}$ to 2.37 $\mu g \cdot m^{-3}$ in 2025, whereas relative urban enhancement declined moderately, from 11.38% to 9.26 %. Decomposition results show that anthropogenic driver overwhelmingly governed the $PM_{2.5}$ reductions and convergence of the $PM_{2.5}$ gap, while meteorological conditions occasionally produced offsetting opposing effects. Interpretation of ML results demonstrate nonlinear meteorological modulation. Mean absolute interquartile contrasts fell from 0.32 $\mu g \cdot m^{-3}$ to 0.19 $\mu g \cdot m^{-3}$ across policy phases, yet measurable meteorological influences persisted even after large-scale gap convergence. Our findings highlight that regional $PM_{2.5}$ reductions do not automatically deliver proportional elimination of urban pollution excess, underscoring the need for integration of meteorological conditions, anthropogenic emission controls and urban-nonurban heterogeneity when developing refined air quality management strategies.

https://doi.org/10.5194/egusphere-2026-6957
Preprint. Discussion started: 23 November 2026
© Author(s) 2026. CC BY 4.0 License.

1 Introduction

Fine particulate matter ($PM_{2.5}$) pollution is a long-standing prominent environmental challenge in China, with significant implications for public health, regional haze and earth's climate (Pope and Dockery, 2006; Guo et al., 2014; Huang et al., 2014; Pui et al., 2014; Shen et al.,2020). Through the early 2000s, rapid industrialization, coal combustion, traffic growth, construction activities, and urban expansion collectively drove elevated $PM_{2.5}$ levels, especially in densely populated and economically developed urban agglomerations (Chan and Yao, 2008; Zhang et al., 2012; Zheng et al., 2018, Ji et al.,2023; Shen et al.,2017). Therefore, since 2013, Chinese government had implemented successive clean-air regulations, including the Air Pollution Prevention and Control Action Plan and the Three-Year Action Plan for Winning the Blue-Sky Defense War, etc. These policies promoted industrial restructuring, coal use reduction, energy substitution, traffic and dust management, plus cross-regional collaborative abatement, leading to substantial $PM_{2.5}$ decreases across many regions of the country (Zheng et al., 2018; Zhang et al., 2019; Chen et al., 2020; Shi et al., 2022; Yu et al., 2022, Lei et al.,2022). However, in highly urbanized regions, a decline in regional mean $PM_{2.5}$ concentrations does not necessarily produce an equivalent reduction in urban-driven pollution (Yun and Zhao, 2022; Liu et al., 2024). This is because that urban expansion alters land use, urban morphology, surface roughness, heat storage, traffic conditions, construction activity, and energy demand, and in turn affects both emission intensities and atmospheric dispersion (Liao et al., 2015; She et al., 2017; Du et al., 2018; Gao et al., 2023).

The Yangtze River Delta (YRD), China, includes dense urban cores, suburban zones, industrial parks, small towns, and rural areas (Liao et al., 2015; She et al., 2017; Zhong et al., 2018). This landscape provides a valuable opportunity to examine how $PM_{2.5}$ differences between urbanized areas and their non-urban surroundings change as regional $PM_{2.5}$ concentrations decline. Some previous studies have examined such urban-nonurban $PM_{2.5}$ contrasts in China. For examples, Liu et al. (2024) investigated urban and nonurban $PM_{2.5}$ changes during 2010-2022 under clean-air interventions with meteorological normalization, while Guo et al. (2025) assessed these differences across typical Chinese cities during 2000-2023. However, the timing, spatial heterogeneity, and meteorological modulation of the urban-nonurban $PM_{2.5}$ gap across successive clean-air policy phases remain less well understood in the YRD. In particular, meteorology can complicate the interpretation of urban-nonurban $PM_{2.5}$ differences. Boundary layer height, wind speed, relative humidity, precipitation, temperature, radiation, cloud cover, and synoptic pressure can modulate $PM_{2.5}$ distributions through vertical mixing, horizontal dispersion, wet removal, secondary formation, and regional transport, etc (Jacob and Winner, 2009; Tai et al., 2012; Yang et al., 2017; Chen et al., 2020). These processes can shape not only regional $PM_{2.5}$ concentrations but also the magnitude of the urban-nonurban contrast. Relationships between meteorological drivers and this gap can be highly nonlinear and differ across regions and pollution-control periods (phases)

Long-term, spatially continuous $PM_{2.5}$ datasets are needed to examine these changes across multiple cities (van Donkelaar et al., 2010; Ma et al., 2016; Xue et al., 2019). Ground-based national monitoring network provides reliable observational data. Nevertheless, its historical time series is comparatively short (starting from 2012), and station coverage is spatially uneven, particularly when aiming to resolve urban and nonurban settlement conditions. In such case, gridded $PM_{2.5}$ products offer a

https://doi.org/10.5194/egusphere-2026-6957
Preprint. Discussion started: 23 November 2026
© Author(s) 2026. CC BY 4.0 License.

more spatially consistent basis for reconstructing long-term urban-nonurban gradients (van Donkelaar et al., 2010; Ma et al., 2016; Xue et al., 2019).

In this regard, here we examined the long-term evolution of the urban-nonurban $PM_{2.5}$ gap across 41 YRD cities from 2000 to 2025. First, the regional, seasonal, and city-scale temporal patterns of the $PM_{2.5}$ gaps were characterized, and their robustness under alternative data-processing configurations were evaluated. We then applied the machine learning (ML) based weather normalization to disentangle contributions of meteorological and anthropogenic drivers to the $PM_{2.5}$ concentrations and gaps, and further utilized the ML approach to analyse roles of different meteorological parameters. This study offers insights into settlement-induced spatial $PM_{2.5}$ disparities amid long-term air-quality improvement and provides supporting evidence for spatially targeted regional air pollution management.

2 Data and methods

2.1 Study area and data sources

2.1.1 Study area

This study focused on the YRD region, one of China's most economically developed, highly urbanized and densely populated regions. Over the past decades, the YRD has undergone rapid urban expansion, accompanied by intensive energy use, and vigorous industrial and transport-related activities. These conditions make it a suitable domain to examine how urban $PM_{2.5}$ varies relative to nonurban surroundings (Li and Wu, 2023). The region covers 41 city-level administrative units: Shanghai Municipality, 13 cities in Jiangsu Province, 11 cities in Zhejiang Province, and 16 cities in Anhui Province (Fig. 1).

2.1.2 $PM_{2.5}$ data and ground-based observations

Monthly $PM_{2.5}$ concentrations were obtained from the 1 km Tracking Air Pollution in China (TAP) gridded product (http://tapdata.org, last accessed: 10 May 2026; Geng et al., 2021; Xiao et al., 2022). The dataset integrates satellite retrievals, in-situ ground observations, chemical transport model simulations, emission inventories, and other auxiliary inputs. The product has undergone comprehensive evaluation by its developers. For the present study, the available TAP record spanned March 2000 to December 2025. The data for January and February 2000 is unavailable, thus the 2000 annual mean was calculated using data from March to December, whereas annual means for 2001-2025 were calculated from complete calendar-year records.

Although the TAP 1 km gridded $PM_{2.5}$ product has been extensively evaluated, we conducted an additional regional assessment using ground-based $PM_{2.5}$ observations from 269 monitoring stations in and around the YRD in 2017. Hourly observations were obtained from the China National Environmental Monitoring Centre and aggregated to monthly means, and then were matched with the corresponding TAP data at each station. The comparison showed very good agreement (Pearson's R^2= 0.90; Fig. S1 in the supplement), providing strong support for the accuracy and reliability of the TAP product used in this work.

https://doi.org/10.5194/egusphere-2026-6957
Preprint. Discussion started: 23 November 2026
© Author(s) 2026. CC BY 4.0 License.

This assessment was only used to validate the TAP data not the urban-nonurban $PM_{2.5}$ gap. Table 1 lists the datasets used in this study (more details in following sections).

Table 1. Overview of main datasets.

Dataset	Data source	Resolution and coverage	Usage in this study
$PM_{2.5}$	TAP 1 km gridded $PM_{2.5}$ product	Monthly, 1 km, 2000-2025	Urban, nonurban, total, and $PM_{2.5}$ gap extraction
Ground observed $PM_{2.5}$	China National Environmental Monitoring Centre (CNEMC)	269 stations; hourly data aggregated to monthly means (2017)	Validation of gridded TAP $PM_{2.5}$ data
Settlement masks	Multi-temporal Global Human Settlement- Settlement Model (GHS-SMOD) classification	Mask epochs: 2000, 2005, 2010, 2015, and 2020; projected 2025 sensitivity	Urban: classes 23 + 30; Nonurban: 11 + 12 + 13 + 21 + 22; Strict nonurban: 11 + 12 + 13
ERA5 meteorology	European Centre for Medium-Range Weather Forecasts Reanalysis version 5 (ERA5) hourly data on single levels	Hourly Coordinated Universal Time (UTC) fields, aggregated into monthly city predictors	Weather normalization and machine-learning analysis
Administrative boundaries	Prefecture-level YRD city boundaries	Total 41 cities in Shanghai, Jiangsu, Zhejiang, and Anhui	City-level extraction and aggregation

2.1.3 Urban and Nonurban settlements

Urban and nonurban pixels were defined using the multi-temporal GHS-SMOD classification (Schiavina et al., 2023; Pesaresi et al., 2024). Following the GHS-SMOD definitions, classes 23 and 30 were grouped as urban, whereas classes 11, 12, 13, 21, and 22 were grouped as the broader nonurban reference (Table S2). To account for urban expansion, the 2000, 2005, 2010, 2015, and 2020 layers were applied to 2000-2004, 2005-2009, 2010-2014, 2015-2019, and 2020-2025, respectively (Table S3). The projected 2025 layer and a stricter nonurban definition restricted to classes 11–13 were used for sensitivity analyses. Raster processing was conducted in ArcGIS 10.8. As shown in Table S4, the urban share of valid YRD pixels increased from 6.35 % (2000 mask) to 9.05 % (2020 mask).

https://doi.org/10.5194/egusphere-2026-6957
Preprint. Discussion started: 23 November 2026
© Author(s) 2026. CC BY 4.0 License.

2.1.4 Meteorological variables

Hourly ERA5 single-level reanalysis data were obtained from the Copernicus Climate Change Service Climate Data Store (CDS; https://cds.climate.copernicus.eu/, last accessed: 5 May 2026) at 0.25° × 0.25° spatial resolution (Hersbach et al., 2020, 2023). The selected variables included 10 m zonal and meridional wind components (U10 and V10), 2 m temperature (T2M), 2 m dew-point temperature (D2M), boundary layer height (BLH), surface solar radiation downwards (SSRD), total precipitation (TP), total cloud cover (TCC), and mean sea-level pressure (MSL). ERA5 fields were spatially compiled for each of the 41 cities and aggregated to monthly values. Wind speed (WS10) was derived from U10 and V10, while relative humidity (RH) was from T2M and D2M. WS10, T2M, RH, BLH, TCC, and MSL were averaged to monthly city-scale means, whereas TP and SSRD were summed to obtain monthly total values.

2.1.5 Policy phases

The study period (2000-2025) was divided into four phases: (N) the pre-control phase (2000–2012), (I) the First Air Pollution Prevention and Control Action Plan period (2013–2017), (II) the Blue Sky Defense War period (2018–2020), and (III) the later improvement and new Action Plan period (2021–2025) (Table 2). This temporal framework was used to compare changes in the urban-nonurban $PM_{2.5}$ gap across successive clean-air policy phases.

Table 2. Definition and introduction of the clean-air policy phases.

Phase	Period	Introduction
N: Pre-control	2000–2012	Baseline before the nationwide $PM_{2.5}$ control policies were fully established
I: First Air Pollution Prevention and Control Action Plan (First Action Plan)	2013–2017	Implementation period of the First Action Plan, featuring strengthened industrial restructuring, coal reduction, traffic and dust control, and regional joint prevention measures
II: Blue Sky Defense War (Second Action Plan)	2018–2020	Three-Year (Second) Action Plan for Winning the Blue-Sky Defense War, featured by continued emission control and regional coordination
III: Later improvement and New (Third) Action Plan	2021–2025	Post-2020 period following Phase II, including the implementation of new (Third) Action Plan released in November 2023

https://doi.org/10.5194/egusphere-2026-6957
Preprint. Discussion started: 23 November 2026
© Author(s) 2026. CC BY 4.0 License.

2.2 Methods

2.2.1 Calculation of urban/nonurban $PM_{2.5}$ metrics

Monthly $PM_{2.5}$ concentrations were calculated separately for urban and nonurban pixel sets within each of the 41 YRD cities. For city i and month t, urban $PM_{2.5}$($U_{i,t}$), nonurban $PM_{2.5}$($N_{i,t}$), their gap ($\Delta PM_{2.5,i,t}$), the pixel-count-weighted combined concentration ($T_{i,t}$), and the pair weight ($w_{i,t}$) were calculated as:

$$U_{i,t} = \left(1/n^{U}{}_{i,t}\right)\sum_{p} \in \Omega^{U}{}_{i,t} PM_{2\cdot 5,p,t} \quad (1)$$

$$N_{i,t} = \left(1/n^{N}{}_{i,t}\right)\sum_{p} \in \Omega^{N}{}_{i,t} PM_{2\cdot 5,p,t} \quad (2)$$

$$\Delta PM_{2\cdot 5,i,t} = U_{i,t} - N_{i,t} \quad (3)$$

$$T_{i,t} = (n^{U}{}_{i,t} U_{i,t} + n^{N}{}_{i,t} N_{i,t})/(n^{U}{}_{i,t} + n^{N}{}_{i,t}) \quad (4)$$

$$w_{i,t} = min(n^{U}{}_{i,t}, n^{N}{}_{i,t}) \quad (5)$$

Where $\Omega^{U}{}_{i,t}$ and $\Omega^{N}{}_{i,t}$ denote the valid urban and nonurban pixel sets, respectively, and $n^{U}{}_{i,t}$ and $n^{N}{}_{i,t}$ are their corresponding pixel counts. Pair weight is defined as the smaller value of urban and nonurban pixel counts and was used in subsequent regional aggregation and weighted modelling. $T_{i,t}$ was used only for weather normalization of regional background.

For seasonal analyses, monthly $\Delta PM_{2.5}$ values were grouped into spring (March-May), summer (June-August), autumn (September-November), and winter (December-February) and aggregated using the same pair-weighting scheme. As a secondary sensitivity metric, relative urban enhancement of a certain year (RE_y) was calculated as $RE_y=(U_y - N_y)/N_y \times 100\%$, where U_y and N_y denote the pair-weighted annual YRD urban and nonurban $PM_{2.5}$ concentrations, respectively. The absolute urban-nonurban $PM_{2.5}$ gap remained the primary metric.

2.2.2 Regional trajectory and breakpoint analysis

Annual YRD urban-nonurban $PM_{2.5}$ gaps were calculated from the city-month $\Delta PM_{2.5}$ values using the pair weights above:

$$\Delta PM^{\mathrm{reg}}_{2.5,y} = \frac{\sum_{i,t\in y} w_{i,t}\Delta PM_{2.5,i,t}}{\sum_{i,t\in y} w_{i,t}} \quad (6)$$

Where y denotes the calendar year， and $w_{i,t}$ is the pair weight defined in Eq. (5).

To identify the possible turning points (breakpoints) before Phase I, continuous segmented linear regression was applied to the annual YRD $\Delta PM_{2.5}$ series for 2000–2012:

$$\Delta PM^{reg}_{2.5,y} = \alpha + \beta_1 t_y + \beta_2 \left(t_y - \tau\right)_{+} + \varepsilon_y \quad (7)$$

where t_y denotes a calendar year, τ is the candidate breakpoint year, $(t_y - \tau)_+ = \max(0, t_y - \tau)$, α is the intercept, β_1 is the slope before the breakpoint, β_2 is the slope change after the breakpoint, and ε_y is the residual error. To avoid selecting breakpoints too close to the boundaries of 2000–2012 period, candidate breakpoints from 2003 to 2009 were evaluated, and the breakpoint

https://doi.org/10.5194/egusphere-2026-6957
Preprint. Discussion started: 23 November 2026
© Author(s) 2026. CC BY 4.0 License.

with the lowest Bayesian Information Criterion (BIC) value was selected. The segmented model was compared with a simple linear model without a breakpoint using the coefficient of determination (R^2), root mean square error (RMSE), corrected Akaike information criterion (AICc), and BIC.

Uncertainties of the breakpoint and segment slopes were assessed using 5000 residual-bootstrap replicates, where the breakpoint was re-estimated within each replicate. The robustness of results was also assessed using alternative breakpoint search windows, parametric bootstrap, and leave-one-year-out (LOYO) refitting.

2.2.3 Weather-normalized decomposition of $PM_{2.5}$ trends

An Least-Squares Boosting (LSBoost)-based weather normalization framework, adapted from previous air quality trend studies (Grange et al., 2018; Qiu et al., 2022), was used to isolate the contribution of meteorological influence from observed $PM_{2.5}$ changes. The analysis was applied to the pixel-count-weighted total $PM_{2.5}$ (T), separately from urban $PM_{2.5}$ (U), nonurban $PM_{2.5}$ (N), and the urban-nonurban gap ($\Delta PM_{2.5}$). For each policy-phase transition, the model was fitted using data from the starting period and then applied to predictor data from both periods. The difference between the resulting predictions for the two periods was used to estimate the meteorological contribution, while the remaining observed change was calculated as the non-meteorological residual. These components were defined as follows:

$$\Delta Y_{s\to e}^{\mathrm{obs}} = \bar{Y}_e - \bar{Y}_s \quad (8)$$

$$\Delta Y_{s\to e}^{\mathrm{met}} = \hat{Y}_s(Z_e) - \hat{Y}_s(Z_s) \quad (9)$$

$$\Delta Y_{s\to e}^{\mathrm{res}} = \Delta Y_{s\to e}^{obs} - \Delta Y_{s\to e}^{met} \quad (10)$$

Where s and e denote the start and end periods, respectively; Y represents T, U, N, or $\Delta PM_{2.5}$; $\bar{Y}_s$ and $\bar{Y}_e$ are the corresponding weighted observed means; and Z_s and Z_e denote the predictor sets of the two periods. The residual, hereafter termed as the anthropogenic driver, represents the observed change that cannot be explained by the meteorological predictors.

For total $PM_{2.5}$, endpoint transitions were assessed for 2000→2012, 2012→2017, 2017→2020, and 2020→2025. For $\Delta PM_{2.5}$, the main analysis used 3-year windows (2001-2003, 2010-2012, 2015-2017, 2018-2020, and 2023-2025), while the corresponding single-year endpoint comparisons were retained as sensitivity analyses. Predictor common support was quantified as the proportion of end-period observations whose meteorological predictor values fall within the range covered by the corresponding start-period training dataset. For these decomposition analyses, LSBoost model included meteorological variables, month, city, and province as predictors. Uncertainty in the decomposition estimates was assessed using city-level cluster bootstrap resampling, with the fitted model held unchanged. In addition, a separate total $PM_{2.5}$ model was trained for each policy phase and then applied to the other phases. The transferred predictions were compared with predictions from a model trained directly on the target phase to assess the stability of the derived $PM_{2.5}$-predictor relationship across different phases. For each prediction phase, we compared the weighted mean prediction from a model trained in another phase with that from the same-phase model. We calculated the relative prediction difference (%) as the absolute difference between the

https://doi.org/10.5194/egusphere-2026-6957
Preprint. Discussion started: 23 November 2026
© Author(s) 2026. CC BY 4.0 License.

two weighted mean predictions, divided by the absolute weighted mean prediction of the same-phase reference model, and multiplied by 100. Larger values indicate greater discrepancies between transferred and same-phase model predictions.

2.2.4 Machine-learning (ML) analysis of meteorological modulation

This separate ML analysis used a pair-weighted LSBoost regression-tree model, with monthly $\Delta PM_{2.5}$ as the response variable. Predictors included the eight meteorological variables described in Section 2.1.4, together with policy phase, month, city, and province; the latter four were treated as categorical variables. Observations were weighted by the minimum valid-pixel support of the urban and nonurban classes. Model hyperparameter were selected via nested training-fold validation, and the final settings are summarized in Table S5.

Model performance was evaluated via random five-fold cross-validation (CV) and LOYO validation. Weighted R^2, RMSE, and MAE (mean absolute error) served as performance metrics. Ridge regression, support vector regression with a radial basis function kernel (RBF-SVR), and Random Forest (RF) were further tested within the same validation framework as supplementary benchmark models (Fig. S2). SHapley Additive exPlanations (SHAP) values were calculated from the fitted LSBoost model to characterize predictor contributions and nonlinear meteorological relationships (Lundberg et al., 2020).

Meteorological modulation of $\Delta PM_{2.5}$ was then quantified using fitted P75-P25 contrasts (P25 and P75 refer to the 25th and 75th percentiles of meteorological variables). This contrast corresponds to the interquartile range, providing a representative measure of variation across the central part of each predictor distribution and reducing sensitivity to extreme values. For each meteorological variable, pooled YRD-wide P25 and P75 values were substituted, while the remaining predictors retained their observed values:

$$C_{r,p,k} = \frac{\sum_{(i,\,t)\in G_{r,p}} w_{i,t}\left[\hat{D}_{i,t}^{\left(k=P_{75,k}\right)} - \hat{D}_{i,t}^{\left(k=P_{25,k}\right)}\right]}{\sum_{(i,\,t)\in G_{r,p}} w_{i,t}} \qquad (11)$$

Where $G_{r,p}$ denotes observations in region r and policy phase p. Negative values indicate smaller fitted urban-nonurban gaps at higher meteorological values. Alternative percentile ranges and region- and phase-specific percentiles were also examined as sensitivity tests.

2.2.5 City-scale slope analysis

To further examine the spatial heterogeneity of urban-nonurban $PM_{2.5}$ gaps, annual $\Delta PM_{2.5}$ values were calculated for each city and year, and city-specific trends were estimated separately in each phase using ordinary least-squares regression:

$$D_{i,y,p} = \alpha_{i,p} + \beta_{i,p} t_y + \varepsilon_{i,y,p} \qquad (12)$$

Where $D_{i,y,p}$ denotes the annual $\Delta PM_{2.5}$ for city i, year y, and phase p; t_y is the in-phase year index; $\alpha_{i,p}$ is the intercept; $\beta_{i,p}$ is the city-specific annual slope, and $\varepsilon_{i,y,p}$ is the residual. A negative $\beta_{i,p}$ value indicates gap narrowing, and *vice versa*.

https://doi.org/10.5194/egusphere-2026-6957
Preprint. Discussion started: 23 November 2026
© Author(s) 2026. CC BY 4.0 License.

3 Results and discussion

3.1 Long-term trend and spatiotemporal heterogeneity of $PM_{2.5}$ concentrations across policy phases

3.1.1 Long-term trends of urban, nonurban $PM_{2.5}$ concentrations and their gap

Based on the pair-weighted dynamic-mask estimates, as shown in Fig. 2, the overall YRD urban $PM_{2.5}$ mass loading increased from 57.19 $\mu g \cdot m^{-3}$ in 2000 to a peak value of 77.01 $\mu g \cdot m^{-3}$ in 2007 and then generally declined to 27.94 $\mu g \cdot m^{-3}$ in 2025. Nonurban $PM_{2.5}$ concentrations were 51.39, 69.14, and 25.57 $\mu g \cdot m^{-3}$ for these three years. The corresponding urban-nonurban gap increased from 5.80 to 7.87 $\mu g \cdot m^{-3}$ then declined to 2.37 $\mu g \cdot m^{-3}$; the long-term trend therefore shifted from early widening toward widespread convergence after 2007. Individually, the four provincial regions showed broadly similar overall narrowing trend, although the magnitude and timing of decline differed slightly across regions. It should be noted that, following the general decline until 2022, a modest rebound can be observed toward 2025 for most regions. At the YRD scale, the gap increased from 1.59 $\mu g \cdot m^{-3}$ in 2022 to 2.98 $\mu g \cdot m^{-3}$ in 2024, before declining to 2.37 $\mu g \cdot m^{-3}$ in 2025. This late increase occurred at a much lower baseline level and varied across the four regions, and did not cancel the long-term convergence tendency identified for the 25-year study period. Overall, Zhejiang retained a comparatively larger urban-nonurban gap in the later phases, whereas Jiangsu showed a smaller gap (Fig. 2). For 2013, the transition year marking the launch of Phase I action, Zhejiang had the lowest urban and nonurban $PM_{2.5}$ concentrations (48.11 and 39.66 $\mu g \cdot m^{-3}$, respectively), yet the largest urban-nonurban gap (8.45 $\mu g \cdot m^{-3}$), slightly exceeding that of Shanghai (8.29 $\mu g \cdot m^{-3}$), with relatively high $PM_{2.5}$ levels. In contrast, Jiangsu and Anhui showed high absolute $PM_{2.5}$ levels (80.30 and 80.45 $\mu g \cdot m^{-3}$, respectively) but much smaller urban-nonurban contrasts (3.45 and 4.17 $\mu g \cdot m^{-3}$, respectively).

As discussed, Figure 2 demonstrates that the annual $PM_{2.5}$ concentrations peaked in 2007, and the data-driven segmented analysis identified 2007 as the best-supported turning point from the 2000–2012 trajectory. The BIC reached its minimum at 2007, supporting the selected breakpoint (Fig. S3; Table S6). Across 5000 residual-bootstrap replicates, 86.4% selected 2007 and 99.8 % identified a breakpoint within 2006–2008. Alternative candidate windows, parametric bootstrap, and LOYO refitting produced consistent breakpoint year (Fig. S3; Table S6). These findings provide strong evidence that the regional transition from a widening to a narrowing urban-nonurban $PM_{2.5}$ gap actually took place several years prior to the 2013 implementation of nationwide action plan. The segmented model was strongly favoured over the no-break linear trend (ΔBIC = 27.69). The fitted slope for $\Delta PM_{2.5}$ changed from +0.24 $\mu g \cdot m^{-3} \cdot yr^{-1}$ before the breakpoint to −0.31 $\mu g \cdot m^{-3} \cdot yr^{-1}$ thereafter.

Moreover, sensitivity analyses using alternative settlement masks, nonurban definitions, weighting schemes, calendar specifications, and year exclusions consistently confirmed the long-term narrowing trend of urban-nonurban $PM_{2.5}$ gap (Fig. S4-S7; Tables S7–S8). Relative urban enhancement (RE) in the YRD showed a moderate decrease, from 11.38% at the 2007 absolute-gap maximum to 9.26% in 2025 (Fig. S8). Thus, the pronounced narrowing of the absolute gap was accompanied by weaker proportional convergence relative to the declining nonurban background levels.

Overall, this timing aligns with previous national and regional studies showing diminishing urban-nonurban $PM_{2.5}$ contrasts throughout China's clean-air era (Liu et al., 2024; Guo et al., 2025). The breakpoint analysis revealed that convergence had

https://doi.org/10.5194/egusphere-2026-6957
Preprint. Discussion started: 23 November 2026
© Author(s) 2026. CC BY 4.0 License.

already begun within the pre-control period, ahead of the 2013 police phase. Our analysis characterizes how this ongoing convergence evolves across successive clean-air phases, rather than attributing its onset to any single policy intervention.

3.1.2 Seasonal variation of the $PM_{2.5}$ gap

Seasonal analysis showed that the long-term urban-nonurban $PM_{2.5}$ convergence occurred across all seasons, not confined to a single season (Fig. 3). For the whole YRD, the gap declined in all four seasons from 2000-2012 to 2013-2017, and further decreased from 2013-2017 to 2018-2020. This general pattern was also observed individually in Shanghai, Jiangsu, Zhejiang, and Anhui, and the pair-weighted dynamic-mask gap remained positive for every region-phase-season combination. The convergence identified in the annual time series was therefore consistently present at both spatial and seasonal scales in YRD. A clear seasonal ranking also persisted at the whole YRD and across the four provincial regions, yet the overall magnitude of the gap declined over time. Summer consistently showed the smallest gap, whereas winter generally yielded the largest. The only exception was Jiangsu in 2013-2017, when spring and winter gaps were nearly identical (3.19 and 3.13 $\mu g \cdot m^{-3}$, respectively). Seasonal contrasts were most obvious during 2000-2012, particularly in Shanghai and Zhejiang: their winter gaps reached 14.86 and 14.49 $\mu g \cdot m^{-3}$, compared with summer values of 7.04 and 6.45 $\mu g \cdot m^{-3}$, respectively. Subsequently, by 2021-2025, winter gaps had declined to 3.40, 1.73, 6.41, and 3.21 $\mu g \cdot m^{-3}$ for Shanghai, Jiangsu, Zhejiang, and Anhui, respectively. Zhejiang therefore maintained the largest winter contrast in the latest phase, even though its magnitude was less than half of its value recorded for 2000-2012.

For the whole YRD, changes between 2018-2020 and 2021-2025 were relatively small, whereas seasonal trajectories differed among the four provincial regions. Zhejiang continued to decline in all four seasons, although its summer gap changed only slightly from 2.54 to 2.50 $\mu g \cdot m^{-3}$. Shanghai and Anhui exhibited mild increases in spring and summer along with further reductions in autumn and winter, whereas Jiangsu showed only a minor summer increase from 0.98 to 1.08 $\mu g \cdot m^{-3}$, with decreases in the other three seasons. It should be noted that, these late-phase fluctuations occurred against a substantially lower baseline gap relative to 2000-2012 and thus did not alter the overall pattern of long-term convergence. This persistent seasonal pattern suggests that the urban-nonurban $PM_{2.5}$ gap continues to vary systematically over the year, even after the substantial convergence.

3.1.3 City-scale spatial heterogeneity of the $PM_{2.5}$ gap

City-specific slopes demonstrating the magnitude of $\Delta PM_{2.5}$ variations, as showed in Fig. 4, revealed clear spatial heterogeneity (detailed values in Table S9). For the 2000-2012 period (Phase N), trends across individual cities were mixed: 19 of the 41 cities had slopes above 0.03 $\mu g \cdot m^{-3} \cdot yr^{-1}$, 7 had slopes below -0.03 $\mu g \cdot m^{-3} \cdot yr^{-1}$ and 15 fell within the range of -0.03 to 0.03 $\mu g \cdot m^{-3} \cdot yr^{-1}$. The average slope across all cities stood at 0.04 $\mu g \cdot m^{-3} \cdot yr^{-1}$. In turn, this spatially variable pattern agreed with the regional trajectory over the same period, which transitioned from an early widening phase toward narrowing after 2007 instead of following a uniform trend across the full 2000–2012 period.

https://doi.org/10.5194/egusphere-2026-6957
Preprint. Discussion started: 23 November 2026
© Author(s) 2026. CC BY 4.0 License.

A more distinct pattern emerged for the 2013-2017 period (Phase I). 26 cities had slopes below -0.03 $\mu g \cdot m^{-3} \cdot yr^{-1}$, of which 23 fell beneath -0.10 $\mu g \cdot m^{-3} \cdot yr^{-1}$, and the mean slope across cities dropped to -0.26 $\mu g \cdot m^{-3} \cdot yr^{-1}$. The steepest declines occurred in Nanjing, Hangzhou, and Changzhou, with slopes of -1.75, -1.44, and -0.95 $\mu g \cdot m^{-3} \cdot yr^{-1}$, respectively. Nevertheless, the convergence of $PM_{2.5}$ gap was not even across all 41 cities, the prevalence of negative slopes indicates that regional narrowing during Phase I extended broadly in space, and was not driven by a few cities only.

The spatial heterogeneity became a bit more scattered after 2018. For the 2018-2020 period (Phase II), 19 cities had slopes below -0.03 $\mu g \cdot m^{-3} \cdot yr^{-1}$, another 19 had slopes above 0.03 $\mu g \cdot m^{-3} \cdot yr^{-1}$, and 3 fell within the -0.03 to 0.03 $\mu g \cdot m^{-3} \cdot yr^{-1}$ interval. The mean slope of all cities was 0.02 $\mu g \cdot m^{-3} \cdot yr^{-1}$. Subsequently, positive slopes became more common during 2021-2025 (Phase III): 32 cities had slopes above 0.03 $\mu g \cdot m^{-3} \cdot yr^{-1}$, 7 had slopes below -0.03 $\mu g \cdot m^{-3} \cdot yr^{-1}$, and 2 fell within -0.03 to 0.03 $\mu g \cdot m^{-3} \cdot yr^{-1}$. The city-average slope increased to 0.17 $\mu g \cdot m^{-3} \cdot yr^{-1}$. Such changes matched with the observations shown in Fig. 2. Importantly, such late-phase positive slopes appeared after the urban-nonurban gap had already declined markedly. Therefore, the results likely indicate a short-term local widening or fluctuation under a low-gap baseline, instead of a solid rebound toward the far stronger contrasts observed in earlier phases.

Taken together, the city-scale results show that regional convergence was neither spatially uniform nor temporally consistent. The most pronounced and spatially widespread narrowing took place over 2013-2017, whereas later phases were characterized by increasing local divergences in trend, despite a substantially small regional gap.

3.2 $PM_{2.5}$ changes with meteorological normalization in different phases

3.2.1 Drivers of overall $PM_{2.5}$ trends

We first conducted the total $PM_{2.5}$ decomposition analysis, and interpreted the drivers across different phases, as shown in Fig. 5 (detailed results are listed in Table S10). The analysis compared the endpoint years of 2000, 2012, 2017, 2020, and 2025, corresponding to the policy-phase boundaries. For Shanghai, Jiangsu, Zhejiang, and Anhui, total $PM_{2.5}$ all increased from 2000 to 2012 and then declined during the three subsequent phases. The magnitude of reduction, however, weakened substantially for 2020-2025. Namely, the regional trend transitioned from rapid post-2012 reductions to a later phase with modest incremental reductions.

To elaborate, during 2000-2012 (Phase N), though $PM_{2.5}$ concentrations declined after peaking in 2007, the level in 2012 remained markedly higher than that in 2000. The decomposition results show that meteorological contributions were mostly negative over this period, indicating they were favourable for $PM_{2.5}$ reduction, especially in Shanghai (-6.05 $\mu g \cdot m^{-3}$), Jiangsu (-8.10 $\mu g \cdot m^{-3}$) and Anhui (-4.96 $\mu g \cdot m^{-3}$). Only Zhejiang showed a slightly positive meteorological contribution (+0.61 $\mu g \cdot m^{-3}$). Notably, the anthropogenic driver was the dominant factor associated with the $PM_{2.5}$ increases across all four regions.

By contrast, from 2012 to 2017 (the transition into Phase I), the trends were totally reversed relative to the pre-control 2000-2012 phase. All four regions experienced substantial declines (30.23 $\mu g \cdot m^{-3}$ in Shanghai, 23.17 $\mu g \cdot m^{-3}$ in Jiangsu, 8.69 $\mu g \cdot m^{-3}$

https://doi.org/10.5194/egusphere-2026-6957
Preprint. Discussion started: 23 November 2026
© Author(s) 2026. CC BY 4.0 License.

^{3} in Zhejiang, and 16.55 μg·m^{-3} in Anhui). By comparison, the contributions from corresponding meteorology were small but positive, ranging from +0.53 to +3.15 μg·m^{-3}, meaning that it was actually not favoured for $PM_{2.5}$ reduction, different from their roles in Phase N. The anthropogenic driver, dominated by emission controls, was instead strongly negative across all regions. The substantial $PM_{2.5}$ reductions were thus overwhelmingly driven by anthropogenic emission cuts, offsetting the minor adverse effect imposed by meteorology. Similarly, using the fitted baseline response functions, meteorology alone could not explain the observed $PM_{2.5}$ decline. In fact, meteorology slightly reduced the net benefits of emission abatement.

Next, from 2017 to 2020 (the transition into Phase II), total $PM_{2.5}$ continued to decrease markedly with observed reductions ranging from 11.59 to 13.79 μg·m^{-3}. However, the meteorological contributions became regionally uneven (from -1.99 to +2.05 μg·m^{-3}): they were positive in Shanghai and Zhejiang but negative in Jiangsu and Anhui, indicating that meteorological driver did not follow the same direction across the four regions. Despite this divergence, and consistent with Phase I, the anthropogenic driver accounted for most of the $PM_{2.5}$ reductions, ranging from −15.36 to −10.04 μg·m^{-3}.

Finally, from 2020 to 2025 (the transition into Phase III), the magnitude of observed $PM_{2.5}$ decreases in all regions became considerably small (0.64–4.73 μg·m^{-3}). Meteorological influence was more spatially variable in both direction and magnitude: they facilitated $PM_{2.5}$ mitigation in Shanghai, Jiangsu, and Anhui (-0.84 to -2.31 μg·m^{-3}), whereas they slightly offset the decline in Zhejiang (+0.37 μg·m^{-3}). Unlike the previous two post-2012 phases, this latest phase exhibited weaker regional consistency in the relative contributions of both meteorological and anthropogenic drivers, along with an overall small $PM_{2.5}$ response. Notably, these changes occurred on the basis of already greatly lowered $PM_{2.5}$ background levels.

These phase-dependent changes are generally similar to prior studies examining meteorological and anthropogenic drivers of air pollution trends. For examples, Zhang et al. (2019) found that population-weighted $PM_{2.5}$ mass loading dropped sharply nationwide during 2013-2017 (Phase I), with anthropogenic emission reductions accounting for 91% of the total change and meteorological factors contributing only 9%. Further, Geng et al. (2024) showed that national $PM_{2.5}$ average concentrations continued to decline during 2018-2020 (Phase II), yet the rate of decrease slowed significantly compared with the 2013-2017 period (Phase I); even so, anthropogenic abatement remained the dominant driver relative to its meteorological companion. Overall, the quantified contributions from anthropogenic and meteorological drivers in these two studies agree closely with our results, which verifies the reliability of our method. In addition, our earlier work (Meng et al. (2025)) examined the elemental carbon (EC) trends and their drivers across four cities in the YRD over 2013-2023. For 2013-2017 and 2018-2020, anthropogenic emission cuts again overwhelmingly dominated EC reductions (91.5-98.5%); during 2021-2023, the EC reduction slowed substantially, but anthropogenic driver remained the leading factor (68.8-177.8%) yet meteorological driver even exerted negative contributions in Nanjing (-7.5%) and Suzhou (-77.8%). It is worth to highlight that both this and the present work adopted the ML-based decomposition method. Such approach has been applied in trend analyses of $PM_{2.5}$ (in other regions) (Ji et al., 2023; Zhang et al., 2023), organic aerosol (Zhang et al., 2026), ozone (Fang et al., 2026; Zhang et al., 2026; Zhu et al., 2024) and volatile organic compounds (VOCs)(Zhu et al.,2024) by our group; it is considerably simpler than previous frameworks that couple emission inventories, chemical transport models, exposure-response functions and cost-benefit assessment models, further demonstrating its practical applicability.

https://doi.org/10.5194/egusphere-2026-6957
Preprint. Discussion started: 23 November 2026
© Author(s) 2026. CC BY 4.0 License.

Furthermore, we conducted the cross-phase transfer analysis to investigate whether the $PM_{2.5}$-driver response relationship derived from one phase can be generalized to other phases. The relative prediction differences (%), which quantify the deviations of transferred model outputs from outputs of the same-phase benchmark model, were shown for all four regions in Fig. 6. The results showed that the fitted total $PM_{2.5}$ response structure was broadly comparable across the four phases, although not fully stable. For most cases, the relative differences remained below 2%, suggesting reasonably similar $PM_{2.5}$ responses across different phases. Relative large deviations close to 5%, however, were observed when comparisons were made between phases with large temporal gaps. For instance, when the 2021-2025 model was applied to the 2000-2012 phase in Zhejiang and Anhui, the deviations reached 4.81% and 4.88%, respectively. But for shanghai, the pair of 2000-2012 and 2021-2025 seemed to perform quite well (0.79% and 1.72%), and the larger deviations appeared in 2000-2012 predictions from 2013-2017 (3.06%) and 2018-2020 (3.2%) trainings. For Jiangsu, the relatively larger errors were from 2018-2020 predictions paired with 2000-2012 (3.76%) and 2021-2025 (3.56%) trainings. Note these differences were also direction-dependent: reversing the training and prediction phases did not generally produce the same deviation. This asymmetry indicates that the fitted relationship between $PM_{2.5}$ and the model predictors changed to some extent as the regional pollution situation evolved.

Overall, the decomposition results (Fig. 5 and Table S10) indicate that the increase in $PM_{2.5}$ during 2000-2012 and the subsequent post-2012 reductions were mainly driven by anthropogenic activities. Cross-phase comparisons (Fig. 6) proved generally similar fitted $PM_{2.5}$-predictor relationships across different policy phases, although relatively larger deviations between time-widely separated phases suggested that these relationships changed as the regional background pollution evolved.

3.2.2 Weather-normalized decomposed changes of $PM_{2.5}$ gap

We adopted the 3-year-window decomposition as the key approach to quantify weather-normalized changes in the urban-nonurban $PM_{2.5}$ gap, and results are shown in Fig. 7 (Table S11). For the whole YRD, very little net change was observed between 2001-2003 and 2010-2012 (only -0.03 $\mu g \cdot m^{-3}$), and contributions of both the meteorological and anthropogenic drivers were nearly zero too. In contrast, a pronounced shift occurred from 2010-2012 to 2015-2017, when the observed gap decreased by 2.18 $\mu g \cdot m^{-3}$. The meteorological contribution was +0.18 $\mu g \cdot m^{-3}$, and the anthropogenic driver was -2.35 $\mu g \cdot m^{-3}$ (95% confidence interval (CI): -3.23 to -1.45 $\mu g \cdot m^{-3}$). The positive meteorological contribution indicates that it slightly widened the urban-nonurban gap, opposite to the observed convergence driven by non-meteorological (anthropogenic) driver. The convergence continued from 2015-2017 to 2018-2020. The observed YRD gap decreased by 1.22 $\mu g \cdot m^{-3}$, of which only -0.07 $\mu g \cdot m^{-3}$ stemming from the meteorological driver and contribution of the anthropogenic driver was -1.15 $\mu g \cdot m^{-3}$ (95 % CI: -1.55 to -0.70 $\mu g \cdot m^{-3}$). By contrast, minor further narrowing across the YRD occurred between 2018-2020 and 2023-2025. The observed change was only -0.18 $\mu g \cdot m^{-3}$, the meteorological driver contributed -0.05 $\mu g \cdot m^{-3}$, and the 95% CI for the anthropogenic driver included zero. The regional trajectory therefore changed from remarkable convergence after 2012 to relative stability in the latest low-gap period.

Province-specific results generally followed a similar trend but varied substantially both in magnitude and persistence (Fig. 7). Shanghai showed the strongest convergence from 2010-2012 to 2015-2017, with an observed decrease of 5.39 $\mu g \cdot m^{-3}$ and an

https://doi.org/10.5194/egusphere-2026-6957
Preprint. Discussion started: 23 November 2026
© Author(s) 2026. CC BY 4.0 License.

anthropogenic-driver contribution of -5.44 $\mu g \cdot m^{-3}$; the gap continued to converge through 2018-2020, and was followed by a slight increase in the most recent time window. Jiangsu showed smaller post-2012 changes, with observed declines of 1.47 and 0.95 $\mu g \cdot m^{-3}$ across the middle two windows, with near-zero net changes after 2018-2020. Zhejiang differed from other regions, as it sustained relatively obvious decreases across all three post-2012 windows; its gap decreased by 2.43 $\mu g \cdot m^{-3}$ from 2010-2012 to 2015-2017, by a further 1.78 $\mu g \cdot m^{-3}$ into 2018-2020, and by another 0.99 $\mu g \cdot m^{-3}$ over the final period. Anhui likewise had the gap narrowed during the two major post-2012 windows, with decreases of 1.43 and 0.94 $\mu g \cdot m^{-3}$, but the gap on the contrary increased by 0.36 $\mu g\ m^{-3}$ from 2018-2020 to 2023-2025. Note anthropogenic drivers remained the dominant factor behind the convergence of urban-nonurban $PM_{2.5}$ gap in Jiangsu, Zhejiang and Anhui, while meteorological drivers had moderate, time-varying influences (relative weak in Jiangsu, and stronger in Zhejiang and Anhui) that sometimes offset or reinforced the anthropogenic influences.

Collectively, as the whole YRD gap shrank, the regional divergence became more apparent. During the two windows after 2012, the four regions generally followed the same trend, while in the latest window, however, their trajectories diverged: Zhejiang continued to narrow, Jiangsu approached stability, while Shanghai and Anhui showed modest widening. The small YRD-wide change after 2018-2020 therefore did not indicate uniform stability across the study domain. Instead, it reflected increasing spatial heterogeneity amid an already largely reduced urban-nonurban contrast of $PM_{2.5}$. In addition, relative to the endpoint-year contrasts, these 3-year windows reduced sensitivity to individual years and provided stronger predictor common support. For the whole YRD, common support values ranged from 0.932 to 0.978 for the 3-year windows, *versus* 0.626 to 0.945 for the corresponding endpoint-year analyses. Moreover, we also carried out endpoint-year sensitivity tests. Although the magnitudes in different periods deviated from the 3-year-window estimates (Fig. S9) in some extent, this alternative analysis generally showed same patterns as identified in Fig. 7.

To further unravel the roles of anthropogenic driver behind the observed convergence, we separately analysed the changes of $PM_{2.5}$ in urban and nonurban settings across different periods using both endpoint-year and three-year window framework (Fig. 8). During phase N (2000-2012), anthropogenic-driven $PM_{2.5}$ increases were found in both urban and nonurban areas, with a larger increase in urban areas. This pattern was in line with the slight widening of the observed urban-nonurban $PM_{2.5}$ gap over the same period (Fig. 2).On the other hand, both urban and nonurban $PM_{2.5}$ displayed remarkable anthropogenic-driven reductions during the two post-2012 windows. Results from the three-year-window analysis (Fig. 8a) showed that from 2010-2012 to 2015-2017, the human-induced change for urban areas was -19.14 $\mu g \cdot m^{-3}$, *versus* -17.19 $\mu g \cdot m^{-3}$ for nonurban $PM_{2.5}$; from 2015-2017 to 2018-2020, the corresponding changes were -14.10 and -13.55 $\mu g \cdot m^{-3}$, respectively. The contributions of urban setting were slightly higher than those of nonurban setting, results from the endpoint-year analysis yielded similar findings (Fig. 8b). The final period showed a different pattern. From 2018-2020 to 2023-2025, the urban and nonurban changes were -6.64 and -6.93 $\mu g \cdot m^{-3}$, respectively. Such close values matched with the minor change in the YRD-wide $\Delta PM_{2.5}$. The disappeared convergence of the gap in this period therefore emerged as the anthropogenic reductions across both urban and nonurban sides became increasingly similar.

https://doi.org/10.5194/egusphere-2026-6957
Preprint. Discussion started: 23 November 2026
© Author(s) 2026. CC BY 4.0 License.

Finally, these urban and nonurban estimates cannot be simply subtracted to derive the corresponding $\Delta PM_{2.5}$, since urban, nonurban, and gap responses were fitted via independent model frameworks, meaning that the values do not obey algebraic additivity. Besides, these values isolate only anthropogenic contributions. Thus, the weather-normalized $\Delta PM_{2.5}$ changes should be derived from the dedicated gap model, instead of subtracting separately urban and nonurban anthropogenic signals.

3.3 Meteorological modulation of the urban-nonurban $PM_{2.5}$ gap

The previous decomposition results demonstrate that the changes in urban-nonurban $PM_{2.5}$ gap could be partially attributed to the meteorological variability. We therefore further examined how meteorological conditions modulated the gap using the weighted LSBoost model. We used this model as the primary model after benchmarking it against ridge regression, RBF-SVR, and RF under the same weighted validation framework. As shown in Fig. S2, the LSBoost implementation achieved a weighted R^2 of 0.882 under five-fold CV, and an RMSE of 1.57 $\mu g \cdot m^{-3}$, an MAE of 1.10 $\mu g \cdot m^{-3}$; its performance remained the best under the LOYO validation, with a weighted R^2 of 0.866, an RMSE of 1.67 $\mu g \cdot m^{-3}$, and an MAE of 1.17 $\mu g \cdot m^{-3}$. Thus LSBoost was chosen as the best model. All 12,710 city-month observational data were retained for model training. This trained LSBoost model was then used to evaluate predictor importance, nonlinear meteorological associations, and their variabilities across regions and policy phases.

3.3.1 Predictor importance and nonlinear meteorological associations

Figure 9a presents the SHAP results describing the importance of spatial, temporal, and meteorological predictors on the urban-nonurban $PM_{2.5}$ gap. City had the largest mean absolute SHAP value (2.21 $\mu g \cdot m^{-3}$), followed by policy phase (1.04 $\mu g \cdot m^{-3}$) and month (0.51 $\mu g \cdot m^{-3}$). These three predictors together accounted for 80.60% of the total summed mean absolute SHAP importance, compared with 19.23% for the eight meteorological variables. This ranking suggests that differences among cities, policy phases, and seasons were the main sources of variation captured by the model, while meteorological conditions contributed additional variability.

Among the meteorological predictors, MSL had the highest mean absolute SHAP value (0.23 $\mu g \cdot m^{-3}$), followed by T2M (0.17 $\mu g \cdot m^{-3}$), BLH (0.15 $\mu g \cdot m^{-3}$), and WS10 (0.11 $\mu g \cdot m^{-3}$). Together, these four variables occupied 73.39% of the meteorological SHAP importance, whereas TCC, TP, RH, and SSRD made smaller contributions. The SHAP distributions in Fig. 9b also showed that individual meteorological variables could have both positive and negative contributions to the fitted gap. Their mean importance thus represent only partial information, as the sign and magnitude of these associations vary with the prevailing meteorological conditions, which therefore warrants further in-depth investigations.

The profiles for BLH and WS10 (Figs. 9e and f) revealed particularly clear nonlinear relationships. SHAP values decreased sharply at relatively low BLH and WS, before approaching flatter responses at higher values. The smoothed curves crossed zero at approximately 466.08 m for BLH and 2.60 $m \cdot s^{-1}$ for WS10. These fitted patterns are consistent with a larger urban-nonurban contrast under shallow boundary layers and weak winds, when atmospheric mixing and dispersion may be less

https://doi.org/10.5194/egusphere-2026-6957
Preprint. Discussion started: 23 November 2026
© Author(s) 2026. CC BY 4.0 License.

effective. However, the zero crossings describe changes in the modelled SHAP contributions rather than physical thresholds, and the fitted relationships cannot independently pinpoint the underlying atmospheric processes.

Other meteorological variables exhibited different response patterns. MSL shifted from negative SHAP contributions at lower pressures to positive contributions at higher pressures (Fig. 9c), whereas T2M presented a generally opposite relationship (Fig. 9d). The SHAP values for TCC and TP also tended to decrease as their values increased (Figs. 9g and h), suggesting smaller fitted urban-nonurban gaps under cloudier or wetter conditions. By comparison, RH and SSRD exhibited weaker and less monotonic relationships (Figs. 9i and j). The differences in their behaviours indicate that meteorological modulation of the urban-nonurban $PM_{2.5}$ gap cannot be adequately summarized by a single linear relationship. Whether these relationships remain consistent across regions and policy phases is examined below.

3.3.2 Regional and phase-specific meteorological contrasts

While the SHAP results describe the overall nonlinear meteorological responses, the strength and sign of these relationships may differ across regions and policy phases. First, the P75-P25 contrasts showed that several meteorological relationships actually retained consistent signs across the 16 region–phase combinations (Fig. 10; Table S12a). Higher BLH, WS10, TP, and TCC were linked with smaller modelled urban-nonurban $PM_{2.5}$ gaps in all combinations, whereas higher RH and MSL were linked to larger gaps throughout. T2M produced a negative contrast in 15 of the 16 combinations, while SSRD showed smaller contrasts with mixed signs.

Directional consistency (namely signs), however, did not translate to unified effect across regions (Fig. 10). Averaged different phases and meteorological variables, the mean absolute fitted contrast was largest in Zhejiang (0.42 $\mu g \cdot m^{-3}$), followed by Shanghai (0.37 $\mu g \cdot m^{-3}$), Anhui (0.17 $\mu g \cdot m^{-3}$), and Jiangsu (0.11 $\mu g \cdot m^{-3}$) (Table S12b). Zhejiang showed particularly large T2M and MSL responses. The T2M contrast reached -1.54 $\mu g \cdot m^{-3}$ in 2013-2017 and -1.74 $\mu g \cdot m^{-3}$ in 2018-2020, while the corresponding MSL contrasts were +0.94 and +0.61 $\mu g \cdot m^{-3}$. Hence, meteorological variables may retain the same directional effect across the YRD, yet their strength of association with the urban-nonurban gap can vary greatly. Another feature of Fig. 10 is the gradual decline in the overall magnitude of modelled meteorological contrasts across policy phases. The mean absolute P75-P25 contrast over the 32 region-variable combinations decreased from 0.32 $\mu g \cdot m^{-3}$ in 2000-2012 to 0.30 $\mu g \cdot m^{-3}$ in 2013-2017, 0.27 $\mu g \cdot m^{-3}$ in 2018-2020, and 0.19 $\mu g \cdot m^{-3}$ in 2021-2025(Table S12c).This downward trend was not same for all variables or regions, though the latest phase clearly situated within a regime of overall weaker contrasts. It should be noted that, this reduction in modelled gaps reflects weaker meteorological responses, but not a complete absence of meteorological modulation. Systematic influences remained even after the absolute urban-nonurban gap narrowed significantly, though the magnitude tended to shrink under the small-gap scenarios of later phases. In fact, sensitivity tests using alternative percentile definitions and region-phase-specific percentile ranges generally reproduced these patterns (Fig. S10; Table S13).

In general, Figs. 9 and 10 manifest that monthly variability was governed by spatial, phase-related, and seasonal patterns, linking strongly with anthropogenic activities, while meteorology exerted a weaker yet systematic, nonlinear modulation.

https://doi.org/10.5194/egusphere-2026-6957
Preprint. Discussion started: 23 November 2026
© Author(s) 2026. CC BY 4.0 License.

Many meteorological associations retained same directional signs across regions and policy-phases, though their modelled magnitudes differed significantly across the YRD and generally declined toward the final low-gap period.

3.4 Uncertainties and limitations

Although the analysis results of trends and drivers are robust supported by several sensitivity analyses, uncertainties remain in the settlement definitions, meteorological decomposition, and model transferability. First, in this work, the nonurban setting covers rural, peri-urban, and semi-dense settlement types and therefore represents a broad settlement background rather than a purely rural or remote area. The absolute value of the urban-nonurban $PM_{2.5}$ gap might be affected by such treatment. A sensitivity analysis using a stricter nonurban definition (GHS-SMOD classes 11–13) indeed yielded larger absolute urban-nonurban $PM_{2.5}$ gaps indeed but retained the same long-term narrowing trend (Fig. S7; Table S7). This proves that the settlement definition affects the estimated magnitude of the gap but does not change the general behaviours of its long-term evolution. In addition, we should also be aware that although the TAP dataset has undergone extensive validation and shows good regional agreement with ground observations in the YRD, the urban-nonurban contrast itself is further derived from the gridded fields and settlement masks, therefore lacks a full observational verification

Second, weather normalization is subject to some uncertainties, including city-level ERA5 representation, predictor common support, model specification, and the incomplete data coverage for the year 2000. In our framework, we quantified the contribution of anthropogenic driver as the portion not captured by the meteorological driver, this treatment may apportion some potentially small signals from meteorology-emission interactions and other unaccounted processes to the anthropogenic activities. Also, the city-cluster bootstrap intervals probably quantify only sampling variability conditional on the fitted model and do not propagate uncertainties originating from the $PM_{2.5}$ gridded product, settlement masks, meteorological fields, or model structure.

Finally, the city-specific slopes for 2018-2020 and 2021-2025 were estimated over relatively short time windows and are therefore descriptive measures of local changes instead of metrics of robust long-term trends. Since Shanghai was treated as a single city-level unit and was not split into finer sub-city units, its city-cluster bootstrap interval failed to capture sub-city uncertainty within Shanghai. Though the bootstrap approach can resolve inter-city uncertainty for Jiangsu, Zhejiang and Anhui, such differences affect the derived province-level estimates of uncertainty. Future insights into the processes influencing the urban-nonurban $PM_{2.5}$ gap may be obtained by using finer spatial observations, aerosol compositional data, emission inventories, and higher-resolution meteorological fields, etc.

4 Conclusions

This work investigated the long-term urban-nonurban $PM_{2.5}$ differences across 41 YRD cities during 2000-2025, based on the 1 km gridded TAP $PM_{2.5}$ products and time-varying settlement classifications. The pair-weighted $PM_{2.5}$ gap increased from 5.80 $\mu g \cdot m^{-3}$ in 2000 to a maximum of 7.87 $\mu g \cdot m^{-3}$ in 2007 and declined thereafter to 2.37 $\mu g \cdot m^{-3}$ in 2025. Segmented

https://doi.org/10.5194/egusphere-2026-6957
Preprint. Discussion started: 23 November 2026
© Author(s) 2026. CC BY 4.0 License.

regressions identified the turning point at 2007, meaning that convergence was already underway before the national clean-air plan launched in 2013. This narrowing trend generally persisted across seasons and alternative settlement classifications. Notably, the relative urban $PM_{2.5}$ enhancement was 11.38% in 2007 and fell moderately to 9.26% in 2025, in contrast to the strong convergence of urban-nonurban $PM_{2.5}$ gap. We applied the weather-normalized decomposition in the long-term trend analysis. Anthropogenic driver was found to dominate $PM_{2.5}$ reductions from 2012 to 2025, while meteorological effects were generally small and, in some regions and phases, even elevated $PM_{2.5}$ levels. Anthropogenic driver also governed convergence of the urban-nonurban $PM_{2.5}$ gap. For instances, the 2.18·μg m^{-3} gap decline between 2010-2012 and 2015-2017 was driven mainly by anthropogenic activities (-2.35 μg·m^{-3}), with a small opposing meteorological contribution (+0.18 μg·m^{-3}); a gap reduction of 1.22 μg·m^{-3} occurred from 2015–2017 to 2018-2020, with an anthropogenic contribution of -1.15 μg·m^{-3}. Furthermore, we explored meteorological modulation on the $PM_{2.5}$ gap using a weighted LSBoost model, which achieved a weighted R^2 of 0.882 in five-fold CV. SHAP analysis showed that city, policy phase and month jointly accounted for 80.6% of total SHAP importance, while meteorological variables contributed the remaining19.2%. Meteorological factors exhibited diverse nonlinear responses; BLH and WS10 showed sharp transitions, though their SHAP zero crossings do not represent physical thresholds. Collectively, the sign of meteorological effects was mostly consistent across YRD regions and phases, but magnitudes differed greatly. The mean absolute meteorological contrast peaked in Zhejiang (0.42 μg·m^{-3}) and was lowest in Jiangsu (0.11 μg·m^{-3}). The average P75-P25 contrast declined from 0.32 to 0.19 μg·m^{-3} across phases, indicating gradually weakening meteorological modulation, while anthropogenic-related factors remained dominant. In future, more studies are needed to resolve region-specific interactions between meteorological conditions and anthropogenic emissions, and assess the stability of these nonlinear relationships under evolving low-pollution regimes, to support spatially refined air quality management in the YRD and other regions.

Code and data availability

The TAP $PM_{2.5}$ data used in this study are available from the Tracking Air Pollution in China platform (http://tapdata.org). The GHS-SMOD settlement data are obtained from the Global Human Settlement Layer (https://doi.org/10.2905/A0DF7A6F-49DE-46EA-9BDE-563437A6E2BA; Schiavina et al., 2023), and ERA5 meteorological data are from the Copernicus Climate Change Service Climate Data Store (https://cds.climate.copernicus.eu/). Ground-based $PM_{2.5}$ observations are from the China National Environmental Monitoring Centre（https://www.cnemc.cn/). The processed data supporting the main results and figures, together with the MATLAB codes used for data analysis and figure generation, are deposited in the Figshare digital repository at [DOI/link].

Supplement

The supplement related to this article is available online.

https://doi.org/10.5194/egusphere-2026-6957
Preprint. Discussion started: 23 November 2026
© Author(s) 2026. CC BY 4.0 License.



Author contributions

NR, ZL and JF contributed to methodology, software, data curation, formal analysis, validation, visualization, and preparation of the original manuscript. XG contributed to conceptualization, methodology, supervision, project administration, and writing – review and editing. ZL and JF contributed to investigation and interpretation of the results. JY, JZ, WL, YZ, MC contributed to discussion of the results and writing – review and editing. All authors reviewed and approved the final manuscript.

Competing interests

The authors declare that they have no conflict of interest.

Financial support

This study was supported by the National Natural Science Foundation of China (grant nos. U24A20515, 42377100 and 42405113).

References

Chan, C. K. and Yao, X.: Air pollution in mega cities in China, Atmos. Environ., 42, 1–42,https://doi.org/10.1016/j.atmosenv.2007.09.003, 2008.

Chen, L., Zhu, J., Liao, H., Yang, Y., and Yue, X.: Meteorological influences on $PM_{2.5}$ and O_3 trends and associated health burden since China's clean air actions, Sci. Total Environ., 744, 140837, https://doi.org/10.1016/j.scitotenv.2020.140837, 2020.

Du, Y., Sun, T., Peng, J., Fang, K., Liu, Y., Yang, Y., and Wang, Y.: Direct and spillover effects of urbanization on $PM_{2.5}$ concentrations in China's top three urban agglomerations, J. Clean. Prod., 190, 72–83, https://doi.org/10.1016/j.jclepro.2018.03.290, 2018.

Gao, G., Pueppke, S. G., Tao, Q., Wei, J., Ou, W., and Tao, Y.: Effect of urban form on $PM_{2.5}$ concentrations in urban agglomerations of China: insights from different urbanization levels and seasons, J. Environ. Manage., 327, 116953, https://doi.org/10.1016/j.jenvman.2022.116953, 2023.

Geng, G., Xiao, Q., Liu, S., Liu, X., Cheng, J., Zheng, Y., Xue, T., Tong, D., Zheng, B., Peng, Y., Huang, X., He, K., and Zhang, Q.: Tracking Air Pollution in China: Near Real-Time $PM_{2.5}$ Retrievals from Multisource Data Fusion, Environ. Sci. Technol., 55, 12106–12115, https://doi.org/10.1021/acs.est.1c01863, 2021.

Geng, G., Liu, Y., Liu, Y., Liu, S., Cheng, J., Yan, L., Wu, N., Hu, H., Tong, D., Zheng, B., Yin, Z., He, K., and Zhang, Q.: Efficacy of China's clean air actions to tackle $PM_{2.5}$ pollution between 2013 and 2020, Nat. Geosci., 17, 987–994, https://doi.org/10.1038/s41561-024-01540-z, 2024.

https://doi.org/10.5194/egusphere-2026-6957
Preprint. Discussion started: 23 November 2026
© Author(s) 2026. CC BY 4.0 License.



Grange, S. K., Carslaw, D. C., Lewis, A. C., Boleti, E., and Hueglin, C.: Random forest meteorological normalisation models for Swiss PM10 trend analysis, Atmos. Chem. Phys., 18, 6223–6239, https://doi.org/10.5194/acp-18-6223-2018, 2018.

Guo, L., Wang, X., Baklanov, A., and Shao, M.: $PM_{2.5}$ Concentration Gap Reduction between Typical Urban and Nonurban China from 2000 to 2023, ACS ES&T Air, 2, 90–98, https://doi.org/10.1021/acsestair.4c00208, 2025.

Guo, S., Hu, M., Zamora, M. L., Peng, J., Shang, D., Zheng, J., Du, Z., Wu, Z., Shao, M., Zeng, L., Molina, M. J., and Zhang, R.: Elucidating severe urban haze formation in China, Proc. Natl. Acad. Sci. U.S.A., 111, 17373–17378, https://doi.org/10.1073/pnas.1419604111, 2014.

Hersbach, H., Bell, B., Berrisford, P., Hirahara, S., Horányi, A., Muñoz-Sabater, J., Nicolas, J., Peubey, C., Radu, R., Schepers, D., Simmons, A., Soci, C., Abdalla, S., Abellan, X., Balsamo, G., Bechtold, P., Biavati, G., Bidlot, J., Bonavita, M., De Chiara, G., et al.: The ERA5 global reanalysis, Q. J. R. Meteorol. Soc., 146, 1999–2049, https://doi.org/10.1002/qj.3803, 2020.

Hersbach, H., Bell, B., Berrisford, P., Biavati, G., Horányi, A., Muñoz Sabater, J., Nicolas, J., Peubey, C., Radu, R., Rozum, I., Schepers, D., Simmons, A., Soci, C., Dee, D., and Thépaut, J.-N.: ERA5 hourly data on single levels from 1940 to present, Copernicus Climate Change Service (C3S) Climate Data Store (CDS), https://doi.org/10.24381/cds.adbb2d47, accessed: 5 May 2026, 2023.

Huang, R. J., Zhang, Y., Bozzetti, C., et al.: High secondary aerosol contribution to particulate pollution during haze events in China, Nature, 514, 218–222, https://doi.org/10.1038/nature13774, 2014.

Jacob, D. J. and Winner, D. A.: Effect of climate change on air quality, Atmospheric Environment, 43, 51–63, https://doi.org/10.1016/j.atmosenv.2008.09.051, 2009.

Ji, Y., Zhang, Y., Liu, D., Zhang, K., Cai, P., Zhu, B., Zhang, B., Xian, J., Wang, H., and Ge, X.: Using machine learning to quantify drivers of aerosol pollution trend in China from 2015 to 2022, Appl. Geochem., 151, 105614, https://doi.org/10.1016/j.apgeochem.2023.105614, 2023.

Lei, R., Nie, D., Zhang, S., Yu, W., Ge, X., and Song, N.: Spatial and temporal characteristics of air pollutants and their health effects in China during 2019–2020, J. Environ. Manage., 317, 115460, https://doi.org/10.1016/j.jenvman.2022.115460, 2022.

Li, S. and Wu, L.: The Effect of Urban Agglomeration Expansion on $PM_{2.5}$ Concentrations: Evidence from a Quasi-natural Experiment, Chin. Geogr. Sci., 33, 250–270, https://doi.org/10.1007/s11769-023-1342-4, 2023.

Liao, J., Wang, T., Jiang, Z., Zhuang, B., Xie, M., Yin, C., Wang, X., Zhu, J., Fu, Y., and Zhang, Y.: WRF/Chem modeling of the impacts of urban expansion on regional climate and air pollutants in Yangtze River Delta, China, Atmos. Environ., 106, 204–214, https://doi.org/10.1016/j.atmosenv.2015.01.059, 2015.

Liu, B., Wang, L., Zhang, L., Bai, K., Chen, X., Zhao, G., Yin, H., Chen, N., Li, R., Xin, J., Wang, Y., Sun, Y., and Hu, B.: Evaluating urban and nonurban $PM_{2.5}$ variability under clean air actions in China during 2010–2022 based on a new high-quality dataset, Int. J. Digit. Earth, 17, 2310734, https://doi.org/10.1080/17538947.2024.2310734, 2024.

https://doi.org/10.5194/egusphere-2026-6957
Preprint. Discussion started: 23 November 2026
© Author(s) 2026. CC BY 4.0 License.



590 Lundberg, S. M., Erion, G., Chen, H., DeGrave, A., Prutkin, J. M., Nair, B., Katz, R., Himmelfarb, J., Bansal, N., and Lee, S.-I.: From local explanations to global understanding with explainable AI for trees, Nat. Mach. Intell., 2, 56–67, https://doi.org/10.1038/s42256-019-0138-9, 2020.

Ma, Z., Hu, X., Sayer, A. M., Levy, R., Zhang, Q., Xue, Y., Tong, S., Bi, J., Huang, L., and Liu, Y.: Satellite-based spatiotemporal trends in $PM_{2.5}$ concentrations: China, 2004–2013, Environ. Health Perspect., 124, 184–192,
595 https://doi.org/10.1289/ehp.1409481, 2016.

Zhang, Q., Zheng, Y., Tong, D., Shao, M., Wang, S., Zhang, Y., Xu, X., Wang, J., He, H., Liu, W., Ding, Y., Lei, Y., Li, J., Wang, Z., Zhang, X., Wang, Y., Cheng, J., Liu, Y., Shi, Q., Yan, L., Geng, G., Hong, C., Li, M., Liu, F., Zheng, B., Cao, J., Ding, A., Gao, J., Fu, Q., Huo, J., Liu, B., Liu, Z., Yang, F., He, K., and Hao, J.: Drivers of improved PM2.5 air quality in China from 2013 to 2017, Proc. Natl. Acad. Sci. U.S.A., 116, 24463–24469, https://doi.org/10.1073/pnas.1907956116,
600 2019.

Meng, Q., Zhang, Y., Zhong, S., Fang, J., Tang, L., Rao, Y., Zhou, M., Qiu, J., Xu, X., Petit, J.-E., Favez, O., and Ge, X.: Technical note: Reconstructing missing surface aerosol elemental carbon data in long-term series with ensemble learning, Atmos. Chem. Phys., 25, 7485–7498, https://doi.org/10.5194/acp-25-7485-2025, 2025.

Zhang, B., Zhang, Y., Zhang, K., Zhang, Y., Ji, Y., Zhu, B., Liang, Z., Wang, H., and Ge, X.: Machine learning assesses
605 drivers of PM2.5 air pollution trend in the Tibetan Plateau from 2015 to 2022, Sci. Total Environ., 878, 163189, https://doi.org/10.1016/j.scitotenv.2023.163189, 2023.

Zhang, Y., Liang, Z., Fang, J., Li, J., Wang, M., Zheng, B., Du, S., Chen, C., Hauglustaine, D., Petit, J.-E., Favez, O., Wang, H., Chen, M., and Ge, X.: Decadal shift in the secondary organic aerosol response to winter haze mitigation in eastern China: Insights from aerosol mass spectrometry measurements and machine learning, Environ. Sci.
610 Technol. Lett., 13, 698–705, https://doi.org/10.1021/acs.estlett.5c01047, 2026.

Fang, J., Zhang, Y., Hauglustaine, D., Zheng, B., Wang, M., Li, J., Sun, Y., Li, H., Wang, J., Wu, Y., Yuan, B., Chen, M., and Ge, X.: Tracking surface ozone responses to clean air actions under a warming climate in China using machine learning, Atmos. Chem. Phys., 26, 851–867, https://doi.org/10.5194/acp-26-851-2026, 2026.

Zhang, K., Zhang, Y., Liang, Z., Fang, J., Gao, Y., Li, H., Li, J., Wang, M., Wang, J., Wu, Y., Ge, X., and Chen, M.:
615 Machine-learning-assisted evaluation of heatwave impacts on surface ozone in China, Intelligent Climate and Eco-Environment, 1, 100008, https://doi.org/10.1016/j.icee.2026.100008, 2026.

Zhu, B., Fang, J., Zhang, Y., Qiu, J., Chen, K., Zhang, K., Liang, H., Yang, H., Ding, Y., and Ge, X.: Machine learning elucidates ubiquity of enhanced ozone air pollution in China linked to the spring festival effect, Atmos. Pollut. Res., 15, 102127, https://doi.org/10.1016/j.apr.2024.102127, 2024.

620 Pesaresi, M., Schiavina, M., Politis, P., Freire, S., Krasnodębska, K., Uhl, J. H., Carioli, A., Corbane, C., Dijkstra, L., Florio, P., Friedrich, H. K., Gao, J., Leyk, S., Lu, L., Maffenini, L., Mari-Rivero, I., Melchiorri, M., Syrris, V., Van Den Hoek, J.,

https://doi.org/10.5194/egusphere-2026-6957
Preprint. Discussion started: 23 November 2026
© Author(s) 2026. CC BY 4.0 License.



and Kemper, T.: Advances on the Global Human Settlement Layer by joint assessment of Earth Observation and population survey data, Int. J. Digit. Earth, 17, 2390454, https://doi.org/10.1080/17538947.2024.2390454, 2024.

Pope III, C. A. and Dockery, D. W.: Health effects of fine particulate air pollution: lines that connect, J. Air Waste Manage. Assoc., 56, 709–742, https://doi.org/10.1080/10473289.2006.10464485, 2006.

Pui, D. Y. H., Chen, S. C., and Zuo, Z.: $PM_{2.5}$ in China: Measurements, sources, visibility and health effects, and mitigation, Particuology, 13, 1–26, https://doi.org/10.1016/j.partic.2013.11.001, 2014.

Qiu, M., Zigler, C. M., and Selin, N. E.: Statistical and machine learning methods for evaluating trends in air quality under changing meteorological conditions, Atmos. Chem. Phys., 22, 10551–10566, https://doi.org/10.5194/acp-22-10551-2022, 2022.

Schiavina, M., Melchiorri, M., and Pesaresi, M.: GHS-SMOD R2023A – GHS settlement layers, application of the Degree of Urbanisation methodology (phase I) to GHS-POP R2023A and GHS-BUILT-S R2023A, multitemporal (1975–2030), European Commission, Joint Research Centre (JRC) [Dataset], https://doi.org/10.2905/A0DF7A6F-49DE-46EA-9BDE-563437A6E2BA, 2023.

She, Q., Peng, X., Xu, Q., Long, L., Wei, N., Liu, M., Jia, W., Zhou, T., Han, J., and Xiang, W.: Air quality and its response to satellite-derived urban form in the Yangtze River Delta, China, Ecol. Indic., 75, 297–306, https://doi.org/10.1016/j.ecolind.2016.12.045, 2017.

Shen, F., Ge, X., Hu, J., Nie, D., Tian, L., and Chen, M.: Air pollution characteristics and health risks in Henan Province, China, Environ. Res., 156, 625–634, https://doi.org/10.1016/j.envres.2017.04.026, 2017.

Shen, F., Zhang, L., Jiang, L., Tang, M., Gai, X., Chen, M., and Ge, X.: Temporal variations of six ambient criteria air pollutants from 2015 to 2018, their spatial distributions, health risks and relationships with socioeconomic factors during 2018 in China, Environ. Int., 137, 105556, https://doi.org/10.1016/j.envint.2020.105556, 2020.

Shi, Q., Zheng, B., Zheng, Y., Tong, D., Liu, Y., Ma, H., Hong, C., Geng, G., Guan, D., He, K., and Zhang, Q.: Co-benefits of CO_2 emission reduction from China's clean air actions between 2013–2020, Nat. Commun., 13, 5061, https://doi.org/10.1038/s41467-022-32656-8, 2022.

Tai, A. P. K., Mickley, L. J., Jacob, D. J., Leibensperger, E. M., Zhang, L., Fisher, J. A., and Pye, H. O. T.: Meteorological modes of variability for fine particulate matter ($PM_{2.5}$) air quality in the United States: implications for $PM_{2.5}$ sensitivity to climate change, Atmos. Chem. Phys., 12, 3131–3145, https://doi.org/10.5194/acp-12-3131-2012, 2012.

Van Donkelaar, A., Martin, R. V., Brauer, M., Kahn, R., Levy, R., Verduzco, C., and Villeneuve, P. J.: Global estimates of ambient fine particulate matter concentrations from satellite-based aerosol optical depth: development and application, Environ. Health Perspect., 118, 847–855, https://doi.org/10.1289/ehp.0901623, 2010.

Xiao, Q., Geng, G., Liu, S., Liu, J., Meng, X., and Zhang, Q.: Spatiotemporal continuous estimates of daily 1 km $PM_{2.5}$ from 2000 to present under the Tracking Air Pollution in China (TAP) framework, Atmos. Chem. Phys., 22, 13229–13242, https://doi.org/10.5194/acp-22-13229-2022, 2022.

https://doi.org/10.5194/egusphere-2026-6957
Preprint. Discussion started: 23 November 2026
© Author(s) 2026. CC BY 4.0 License.



Xue, T., Zheng, Y., Tong, D., Zheng, B., Li, X., Zhu, T., and Zhang, Q.: Spatiotemporal continuous estimates of $PM_{2.5}$ concentrations in China, 2000–2016: A machine learning method with inputs from satellites, chemical transport model, and ground observations, Environ. Int., 123, 345–357, https://doi.org/10.1016/j.envint.2018.11.075, 2019.

Yang, Q., Yuan, Q., Li, T., Shen, H., and Zhang, L.: The relationships between $PM_{2.5}$ and meteorological factors in China: seasonal and regional variations, Int. J. Environ. Res. Public Health, 14, 1510, https://doi.org/10.3390/ijerph14121510, 2017.

Yu, Y., Dai, C., Wei, Y., Ren, H., and Zhou, J.: Air Pollution Prevention and Control Action Plan substantially reduced $PM_{2.5}$ concentration in China, Energy Econ., 113, 106206, https://doi.org/10.1016/j.eneco.2022.106206, 2022.

Zhang, Q., He, K., and Huo, H.: Policy: Cleaning China's air, Nature, 484, 161–162, https://doi.org/10.1038/484161a, 2012.

Zheng, B., Tong, D., Li, M., Liu, F., Hong, C., Geng, G., Li, H., Li, X., Peng, L., Qi, J., Yan, L., Zhang, Y., Zhao, H., Zheng, Y., He, K., and Zhang, Q.: Trends in China's anthropogenic emissions since 2010 as the consequence of clean air actions, Atmos. Chem. Phys., 18, 14095–14111, https://doi.org/10.5194/acp-18-14095-2018, 2018.

Zhong, S., Qian, Y., Sarangi, C., Zhao, C., Leung, R., Wang, H., Yan, H., et al.: Urbanization effect on winter haze in the Yangtze River Delta region of China, Geophys. Res. Lett., 45, 6710–6718, https://doi.org/10.1029/2018GL077239, 2018.

https://doi.org/10.5194/egusphere-2026-6957
Preprint. Discussion started: 23 November 2026
© Author(s) 2026. CC BY 4.0 License.

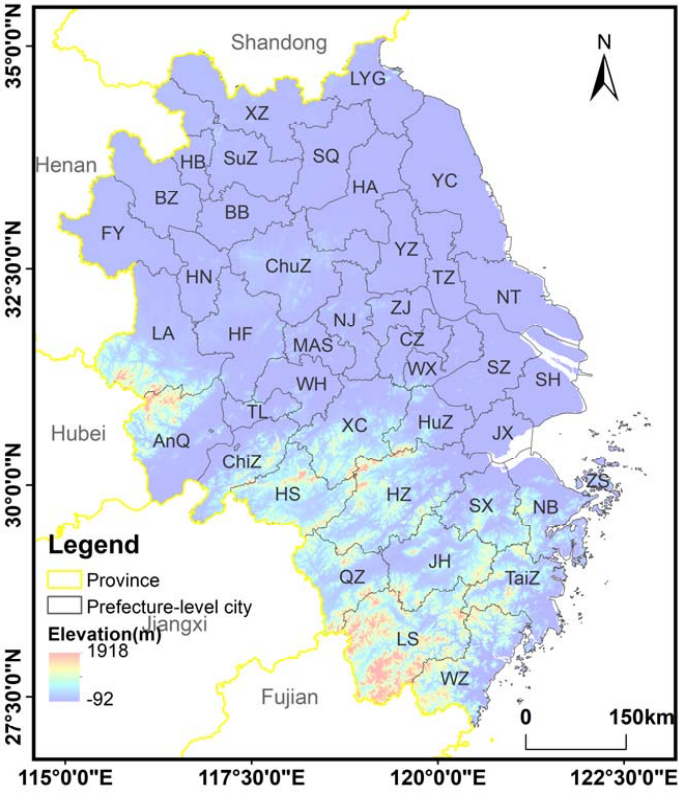

Figure 1. Administrative boundaries, geographical location, and elevation of the study area.

Note: The base map follows standard map GS(2019)1822, with boundaries unchanged, and is also used in Fig. 4. Full city names are listed in Table S1.

https://doi.org/10.5194/egusphere-2026-6957
Preprint. Discussion started: 23 November 2026
© Author(s) 2026. CC BY 4.0 License.

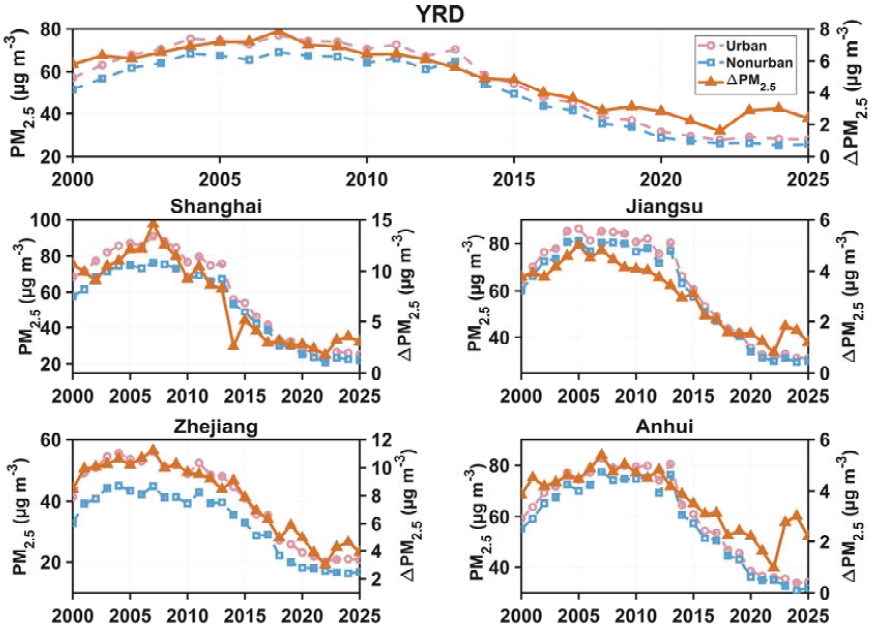

680

Figure 2. Pair-weighted urban and nonurban $PM_{2.5}$ concentrations and their gap ($\Delta PM_{2.5}$ = urban − nonurban) across the YRD and four provincial-level regions during 2000–2025. $PM_{2.5}$ concentrations and urban-nonurban gaps are plotted on separate y-axes.

https://doi.org/10.5194/egusphere-2026-6957
Preprint. Discussion started: 23 November 2026
© Author(s) 2026. CC BY 4.0 License.

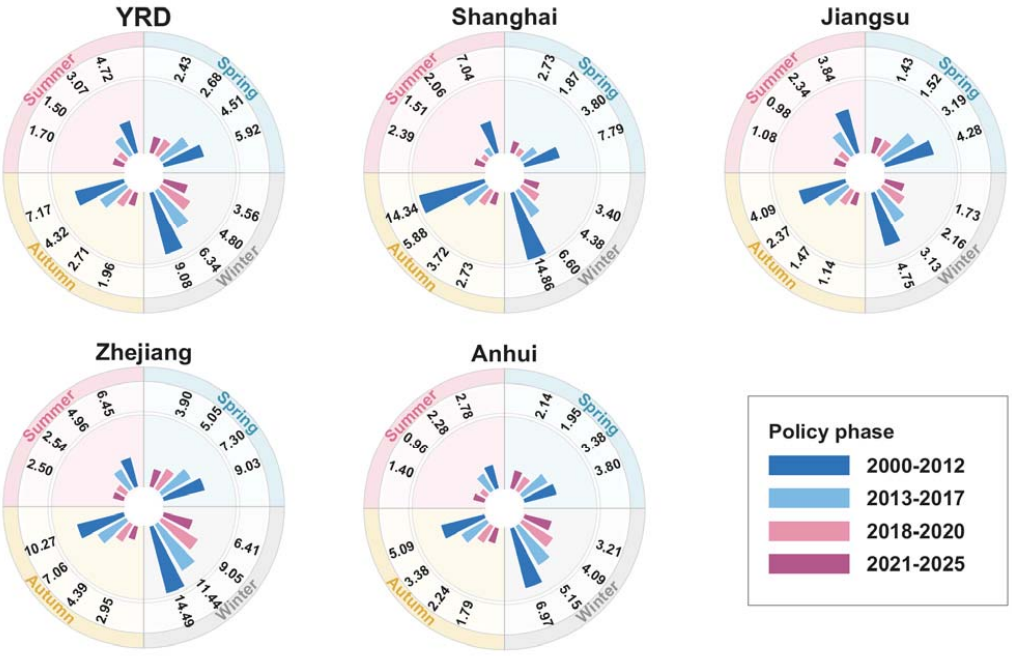

685 **Figure 3. Seasonal pair-weighted urban-nonurban $PM_{2.5}$ gaps across the YRD and four provincial-level regions during the four policy phases.**

https://doi.org/10.5194/egusphere-2026-6957
Preprint. Discussion started: 23 November 2026
© Author(s) 2026. CC BY 4.0 License.

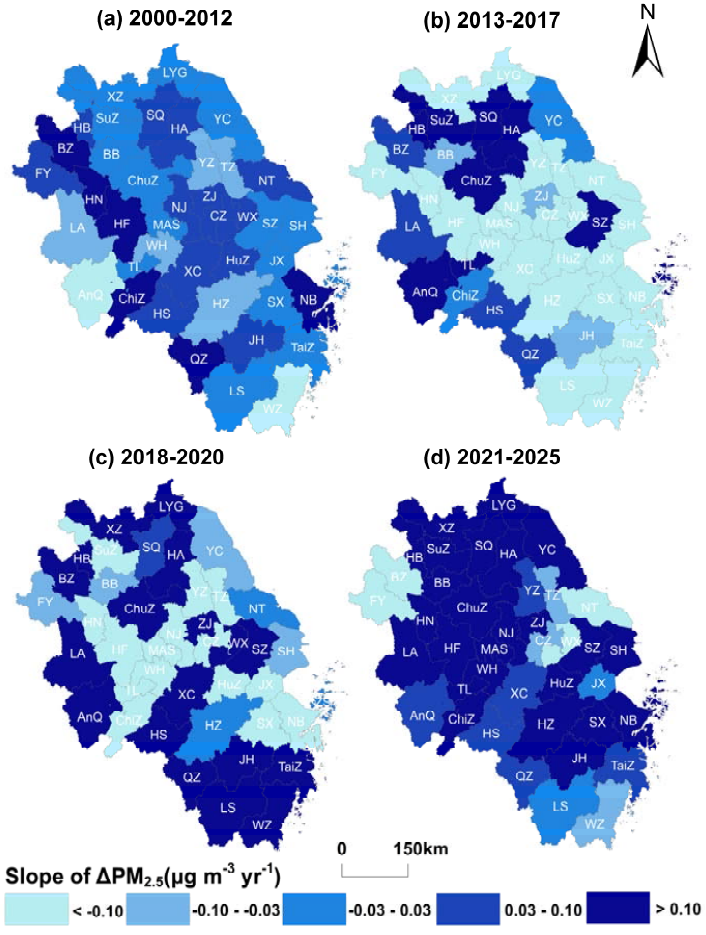

Figure 4. Spatial distribution of city-specific annual slopes of the urban-nonurban $PM_{2.5}$ gap across four policy phases: (a) 2000–2012 (Phase N), (b) 2013–2017 (Phase I), (c) 2018–2020 (Phase II), and (d) 2021–2025 (Phase III).

https://doi.org/10.5194/egusphere-2026-6957
Preprint. Discussion started: 23 November 2026
© Author(s) 2026. CC BY 4.0 License.

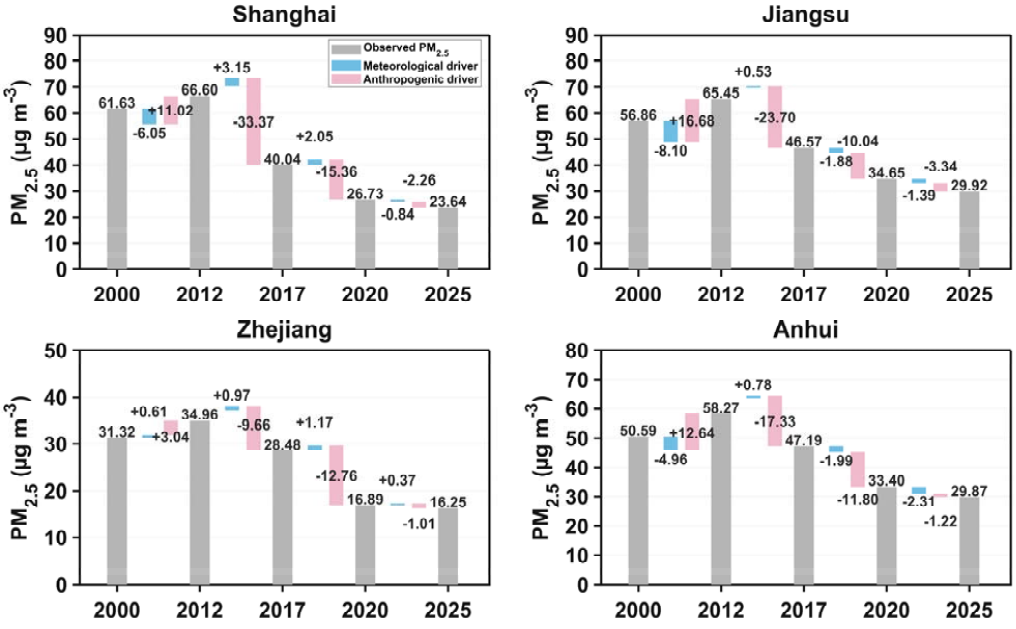

690

Figure 5. Endpoint-year weather-normalized decomposition of total $PM_{2.5}$ changes in the four provincial-level regions over 2000–2025.

https://doi.org/10.5194/egusphere-2026-6957
Preprint. Discussion started: 23 November 2026
© Author(s) 2026. CC BY 4.0 License.

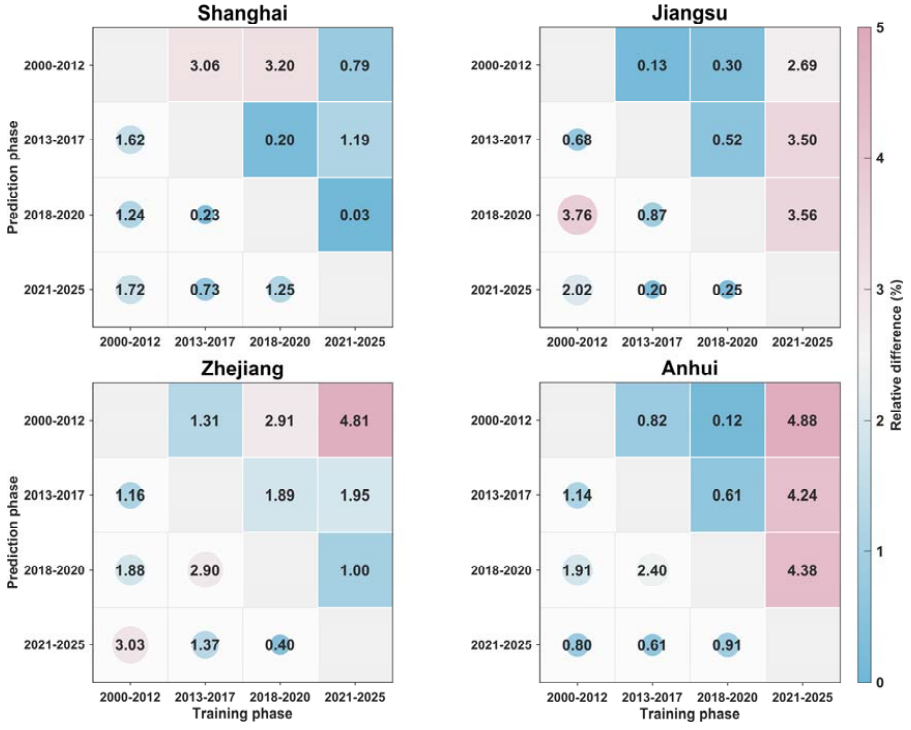

695 **Figure 6. Cross-phase transfer diagnostics for weather-normalized total $PM_{2.5}$ models across the four provincial-level regions. Cell values indicate the absolute relative differences (%) between predictions from transferred models and those from the corresponding same-phase reference models.**

https://doi.org/10.5194/egusphere-2026-6957
Preprint. Discussion started: 23 November 2026
© Author(s) 2026. CC BY 4.0 License.

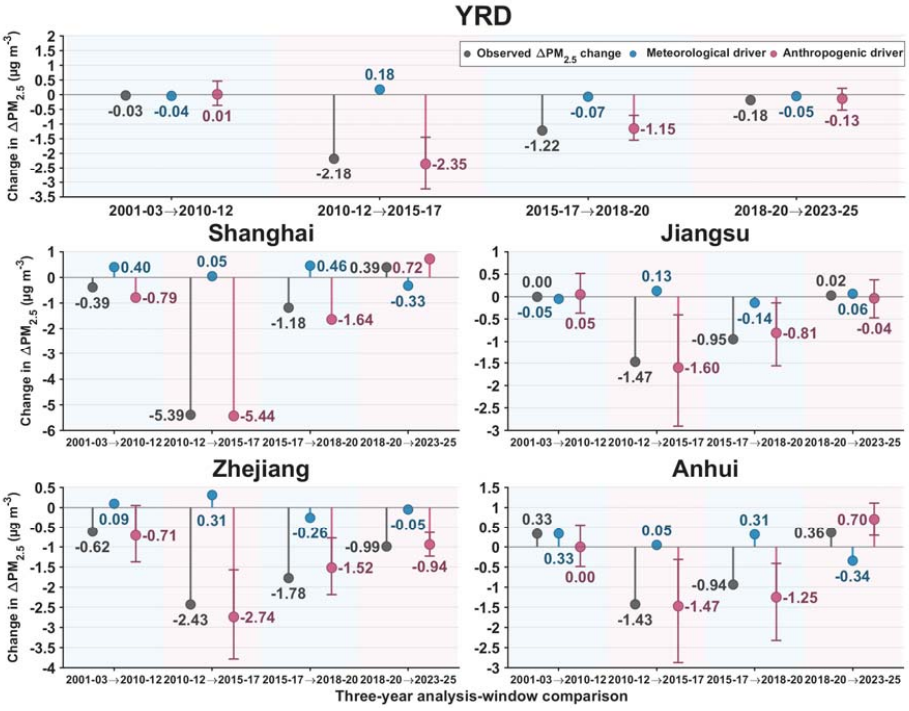

Figure 7. Three-year-window weather-normalized decomposition of changes in the urban-nonurban $PM_{2.5}$ gap across the YRD and four provincial-level regions. Error bars indicate 95 % city-cluster bootstrap confidence intervals (CIs) for the anthropogenic driver.

https://doi.org/10.5194/egusphere-2026-6957
Preprint. Discussion started: 23 November 2026
© Author(s) 2026. CC BY 4.0 License.

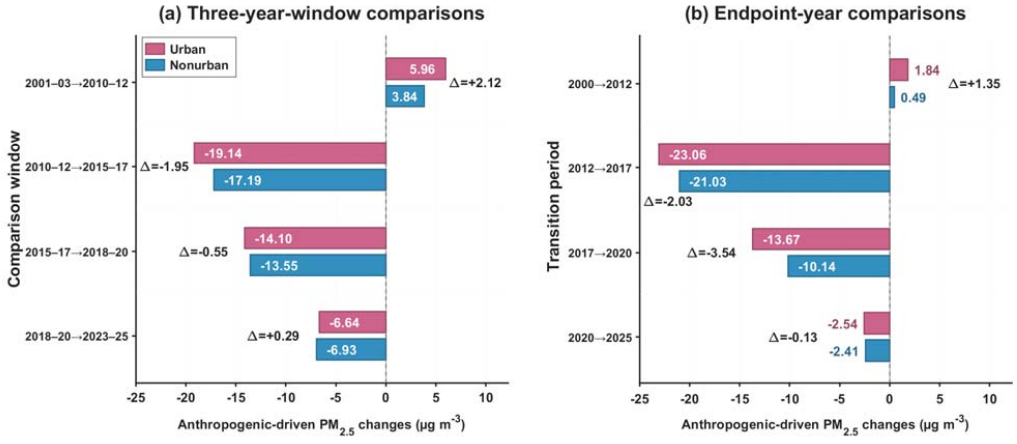

Figure 8. Contributions of the anthropogenic driver to $PM_{2.5}$ changes in urban and nonurban areas across the YRD. Panel (a) shows three-year-window comparisons, and panel (b) presents endpoint-year comparisons.

https://doi.org/10.5194/egusphere-2026-6957
Preprint. Discussion started: 23 November 2026
© Author(s) 2026. CC BY 4.0 License.

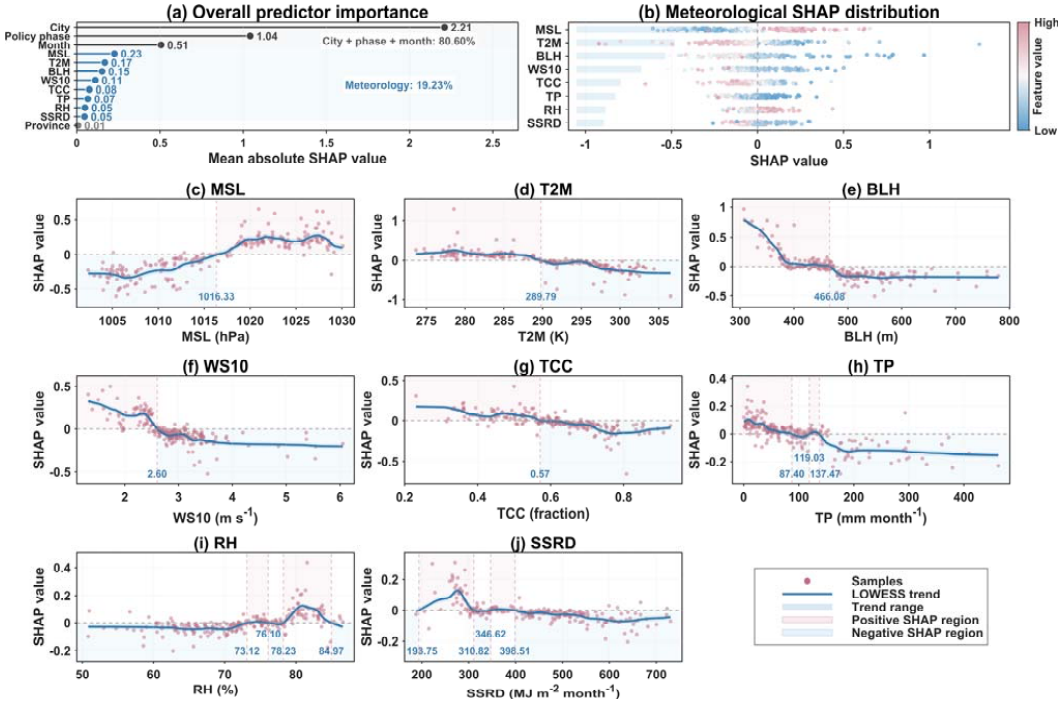

Figure 9. SHAP interpretation for the optimised weighted LSBoost model of urban-nonurban $PM_{2.5}$ gaps. Panel (a) shows the mean absolute SHAP values for all predictors, and panel (b) presents SHAP distributions of the eight meteorological variables. Panels (c–j) display smoothed SHAP dependence relationships for individual meteorological predictors.

720

https://doi.org/10.5194/egusphere-2026-6957
Preprint. Discussion started: 23 November 2026
© Author(s) 2026. CC BY 4.0 License.

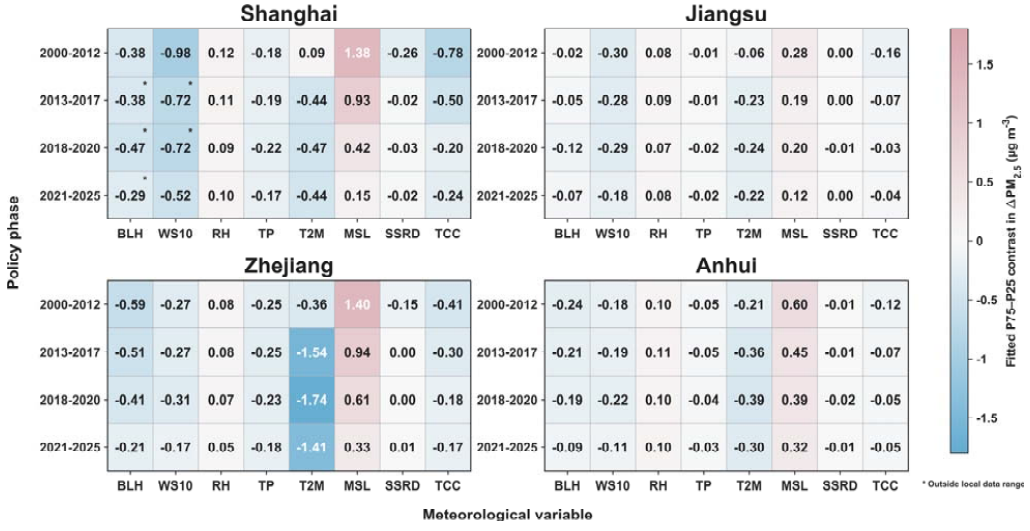

Figure 10. Machine learning (ML)-derived P75-P25 contrasts for the urban-nonurban $PM_{2.5}$ gap across eight meteorological variables, four provincial-level regions, and four policy phases. Asterisks mark cases where at least one pooled percentile lies outside the predictor range for the corresponding region–phase group.